Physics-based unsupervised learning of vortex-induced vibrations from riser field experimental stain data.

Andreas P. Mentzelopoulos [a], Dixia Fan [b], Themistocles Resvanis[a], Themistoklis Sapsis [a], Michael S. Triantafyllou [a]
[a] Department of Mechanical Engineering, Massachusetts Institute of Technology, Cambridge, MA 02139, USA
[b] School of Engineering, Westlake University, Hangzhou, Zhejiang 310024, China

ABSTRACT

We show how to reconstruct the vortex-induced vibrations of a riser from experimental strain measurements using a machine learning framework. We employ a modal decomposition technique followed by inference of the expansion modes using a two-stage optimization routine. A stochastic mode search algorithm is developed and its capabilities and limitations are demonstrated using the MIAMI II riser field experiments, conducted in the Gulf Stream off the coast of Miami, FL using a densely instrumented riser model. Validation is done according to a k-fold cross-validation scheme, and a VIV physics-based examination is presented. The reconstruction framework's complexity in terms of data required for successful training is finally evaluated.

KEY WORDS: Flexible body vortex induced vibrations (VIV); marine riser, unsupervised learning; optimization; optimal sparse modal expansion; stochastic mode search; riser motion reconstruction

INTRODUCTION

Vortex induced vibrations (VIV) are driven by the periodic shedding of vortices formed in the wake behind bluff bodies placed within currents (Triantafyllou et al., 2016). The vibration amplitude does not typically exceed one to two body diameters (Bernitsas et al., 2019). Rigid cylinder VIV have become the canonical problem for study of the phenomenon (Williamson and Roshko, 1988; Wu et al., 2014; Zdravkovich, 1996). Flexible body VIV are similar to rigid body vibrations as they are driven by vortex sheeding, but with the added complexity that the loading is non-uniform along the span as the flexible body undergoes spatially traveling and/or standing waves.

Riser motion reconstruction has been done by leveraging the physics-based modal expansion technique (Mukundan, 2008; Triantafyllou et al., 1999; Wang et al., 2019) developed to model vibrations of continuous flexible bodies, such as beams (Rao, 1995). In this work, the modal expansion approach is employed, followed by a data-informed selection of the expansion modes to restrict the model's complexity while satisfying the motion constraints imposed by VIV physics. The challenge is that a large number of parameters are involved in riser modeling, a problem which is common within the field of regression and has led to a variety of techniques for variable subset selection (Guyon and Elisseeff, 2003). This framework is used to satisfy physics-based VIV motion constraints (for example, amplitude restriction), while still utilizing the modal decomposition model.

METHODS

Data Description

We outline the method using a comprehensive set of field data: The MIAMI II experiments were high mode number VIV experiments conducted in the Gulf Stream off the coast of Miami, FL in 2006. A composite pipe of length $L = 152.524$ m and outer diameter $D = 0.0363$ m was used. The experimental setup is shown in Fig. 6.

The riser was equipped with strain measuring fibers providing strain data at seventy locations along the span (uniformly spaced, excluding the endpoints) every $\Delta z = 2.1335$ m. Measurements were sampled at 50.4857 Hz. Details of the procedures as well as insights gained from the experiments can be found in (Jaiswal and Vandiver, 2007; Jhingran and Vandiver, 2007; Marcollo et al., 2007; Swithenbank and Vandiver, 2007). The data are open-sourced by Prof. Kim Vandiver of MIT and can be accessed through the MIT VIV data repository. For this work, cross-flow strain data collected from experiment No. 20061020164517 between times 50-60 s are used.

Amplitude Reconstruction

Modelling the flow induced motions

Consider a flexible riser of radius R and length L. For cross-flow VIV we expect sinusoidal mode shapes with time varying amplitudes (Mukundan, 2008). Accordingly those may be modelled by Equation 1.

$$y(z,t) = \alpha_0(t) + \sum_{n \in \boldsymbol{S}} \left[\alpha_n(t)\ \cos(\frac{n\pi}{L} z) + \beta_n(t)\ \sin(\frac{n\pi}{L} z) \right] \tag{1}$$

where the contributing expansion modes are in set $\boldsymbol{S} \neq \mathbb{N}_+$ and the coefficients $\alpha_n(t)$ and $\beta_n(t)$ are time dependent functions. We note that Equation 1 is one out of many choices for modelling VIV motions; for example an expansion in terms of orthogonal polynomials could be considered. That would be especially recommended if excessive Gibbs overshooting is observed; other functions may be appropriate depending on the riser properties and the VIV response. We note, for example, that Equation 1 will have a finite number of terms, hence, even if the frequency response is band-limited, accuracy depends on how well the sine and cosine terms describe the response of the riser. For example, traveling waves require a large number of terms, even when the frequency is monochromatic. For simplicity, one may rewrite Equation 1 as follows.

$$y(z,t) = \mathrm{Re}\Big[\sum_{n\in\mathbb{S}} c_n(t)\exp(\frac{in\pi}{L}z)\Big] \tag{2}$$

where i is the imaginary unit and the real symmetric set $\mathbb{S} = \{-\boldsymbol{S}\cup\{0\}\cup\boldsymbol{S}\}$ replaces set $\boldsymbol{S}$. For a riser with circular cross-section the strain in the CF direction measured on the riser's surface may be related to its curvature as follows (Mukundan, 2008).

$$\kappa(z,t) = \frac{\varepsilon_{CF}(z,t)}{R} \approx \frac{\partial^2 y(z,t)}{\partial z^2} = \mathrm{Re}\left[\sum_{n\in\mathbb{S}} -(\frac{n\pi}{L})^2 c_n(t)\exp(\frac{in\pi}{L}z)\right] \tag{3}$$

where ε_{CF} is the CF strain, R is the riser's radius, and κ is the riser's curvature. Equation 3 may be used to determine riser motions given an analytical expression for the strain or vice versa. In addition, it may be used to formulate a system of linear equations to determine the coefficients $c_n(t)$ assuming the set $\mathbb{S} \neq \mathbb{N}_+$ is known a priori and only partial data (i.e. limited measurements) of the strain are available. The least squares problem formulation is as follows.

$$c_n(t_0) = \arg\min_{c_n}\Big\{\sum_{z_i=0}^{z_i=L}\{\mathrm{Re}\left[\sum_{n\in\mathbb{S}} -(\frac{n\pi}{L})^2 c_n\exp(\frac{in\pi}{L}z_i)\right] - \frac{\varepsilon_{CF}(z_i,t_0)}{R}\}^2\Big\} \tag{4}$$

where $n \in \mathbb{S} \neq \mathbb{N}_+$.

Machine-learning the motions of VIV

Let the true riser VIV motions, i.e. the CF displacement as a function of span and time, be

$$g(z,t) \quad \forall z\in[0,L],\ t\in[0,T] \tag{5}$$

and for a single time instant t_0 define $G(z) := g(z,t_0), \forall z \in [0,L]$. From equation 3 it follows that at an instance t_0

$$\frac{d^2G(z)}{dz^2} = \frac{\varepsilon_{CF}(z,t_0)}{R} \Longrightarrow \int_L \left|\frac{d^2G(z)}{dz^2} - \frac{\varepsilon_{CF}(z,t_0)}{R}\right| dz = 0 \tag{6}$$

and more generally since Equation 6 holds true for any $t_0 \in [0,T]$

$$\int_t\int_L \left|\frac{\partial^2 g(z,t)}{\partial z^2} - \frac{\varepsilon_{CF}(z,t)}{R}\right| dz\,dt = 0 \tag{7}$$

for the the flexible riser undergoing VIV.

Let the function $y(z,t)$ be used as a trial function to approximate $g(z,t)$ provided there are limited strain measurements in discrete time instances. Let there be a total of T "snapshots" of the riser represented by the discrete time variable $t \in \{1,2,...,T\}$. Define $Y(z) := y(z,t_0)$ at time instance t_0. We begin by considering Equation 6 for a single time instance, say t_0 without loss of generality. Ideally,

$$Y(z) = G(z) \Longrightarrow \int_L \left|\frac{d^2Y(z)}{dz^2} - \frac{\varepsilon_{CF}(z,t_0)}{R}\right| dz = 0 \tag{8}$$

Equation 8 thus may be used to define and quantify the approximation quality of $Y(z)$ in terms of approximating the true motions $G(z)$ at time instance t_0 by measuring the deviation of the integral expression from zero. We note that we are interested in the magnitude of the deviation only. Extending our approximation quality definition across all time instances, an objective function measuring approximation quality for $y(z,t)$ in terms of approximating $g(z,t)$ may be formulated as follows.

$$\mathbf{J}(y = f(z,t)) = \sum_t \int_L \left|\frac{\partial^2 y(z,t)}{\partial z^2} - \frac{\varepsilon_{CF}(z,t)}{R}\right| dz \tag{9}$$

According to Equation 9, the better the approximation quality, the closer the value of the objective function to zero. We have thus posed the riser motion reconstruction problem as an optimization for which we further need to determine appropriate constraints. We note that Equation 9 is general in the sense that it is applicable without making any assumptions on the form of the trial function $y(z,t)$; however, we underscore that satisfying Equation 9 is not sufficient to optimally approximate the riser's VIV motions, we further need to satisfy VIV physics-based constraints.

At this point, consider the VIV model illustrated in section "Modelling the flow induced motions". In this case the trial function $y(z,t)$ is defined in Equation 2 and the function $Y(z)$ assumes the form

$$Y(z) = y(z,t_0) = \mathrm{Re}\Big[\sum_{n\in\mathbb{S}} c_n(t_0)\ \exp(\frac{in\pi}{L}z)\Big] \tag{10}$$

and represents the trial function at a single time instance, t_0. We note that learning the coefficients $c_n(t_0)$ is a trivial ordinary least-squares (OLS) problem which nonetheless must be repeated at every time instance $t_0 \in \{1,2,...,T\}$. However, learning the expansion modes, i.e. the discrete set $\mathbb{S}$, is the problem of interest. Combining Equations 2 and 9 we obtain the following objective which may be used to learn the set $\mathbb{S}$, containing the modes of the expansion.

$$\mathbf{J}(\mathbb{S}) = \sum_t \int_L \left|\mathrm{Re}\left[\sum_{n\in\mathbb{S}} -(\frac{n\pi}{L})^2 c_n(t)\exp(\frac{in\pi}{L}z)\right] - \frac{\varepsilon_{CF}(z,t)}{R}\right| dz \tag{11}$$

Equation 11 defines an objective which may be used to infer the unknowns of the trial function $y(z,t)$ which assumes the form of Equation 2, subject to the constraint that the coefficients $c_n(t)$ are optimal (least squares sense) at each time instance t_0. A final remark is that both the coefficients $c_n(t)$ and the set $\mathbb{S}$ are learned from the data; however we note that the optimality of the coefficients $c_n(t)$ can only be defined after a choice for the set $\mathbb{S}$ is made. In addition, the coefficients $c_n(t)$ are not learned according to Equation 11 but are determined at each recorded time instance by solving an OLS problem.

Regularization

For the purposes of our trial function a regularization term penalizing high modes modes as well as restricting the number of modes selected can be beneficial; the latter penalty is introduced to restrict the model's complexity. In this case the regularization may assume the following form.

$$\boldsymbol{R}(y(z,t;\mathbb{S})) = \kappa\cdot|s| + \lambda\cdot|\mathbb{S}|, \quad \kappa,\lambda\in\mathbb{R}^+ \tag{12}$$

where the operator $|\cdot|$ indicates cardinality and the factors κ and λ are chosen arbitrarily. The set $s \subset \mathbb{S}$ is a strict subset of $\mathbb{S}$ defined as follows.

$$s = \{s_i \in \mathbb{S} \,\big|\, s_i > n, n \in \mathbb{S}\} \tag{13}$$

where the number $n > 0$ is chosen arbitrarily.

Constraints

Constraints are imposed by the natural phenomenon's physics. The obvious constraint of $y(z,t)$ are the boundary conditions (BCs) of the riser. In the MIAMI II experiments, the top end was pinned while a clump

weight was placed at the bottom of the riser. The pinned BC at the top was implemented as a hard constraint.

$$y(0,t) = 0 \quad \forall t \in [0,T] \tag{14}$$

In addition, assuming the riser can be modelled as in (Triantafyllou et al., 1999), a formulation similar to that of a beam with variable mass and geometric properties, then the bending moments at the ends should be zero (as well as the third derivative of the displacement). Thus,

$$\left.\frac{\partial^2 y(z,t)}{\partial z^2}\right|_{z=0} = \left.\frac{\partial^2 y(z,t)}{\partial z^2}\right|_{z=L} = \left.\frac{\partial^3 y(z,t)}{\partial z^3}\right|_{z=L} = 0 \quad \forall t \in [0,T] \tag{15}$$

The constraints posed by Equation 15 were implemented as soft constraints (by adding zeros as the strain boundary values). Finally, the motions were restricted to approximately one diameter (Bernitsas et al., 2019; Triantafyllou et al., 1999) .

$$\frac{|y(z,t)|}{D} < 1.5 \quad \forall z \in [0,L], t \in [0,T] \tag{16}$$

where D is the cylinder's diameter. Lastly, given that the expected physical vibration mode was not exceeding 30, the expansion modes in S were narrowed down to $\mathbb{S} \subseteq \Omega$, where $\Omega = \{1,2,3,...,90\}$.

Optimization Routine

Optimizing the objective function (Equation 11 plus regularization) in order to obtain the optimal set $\mathbb{S}$ is nontrivial. Essentially, the choice of $\mathbb{S}$ fundamentally alters the nature of $y(z,t)$ as defined in Equation 2 by governing the number of terms used. Formulating a gradient with respect to the unknown parameters is not possible and in addition the parameter space, i.e. cardinality of $\mathbb{S}$ is not fixed. To make maters worse, the number of subsets of Ω are $2^{|\Omega|} = 2^{90}$ which is inexhaustibly large.

A two stage stochastic search approach was employed to minimize the objective. The method is similar to a random search which eventually is informed of previous outcomes. In the first stage, the cardinality of $\mathbb{S}$ was restricted (to some different value at each iteration) and the set $\mathbb{S}$ was drawn uniformly at random from Ω. This stage was the "space exploration" stage. Mathematically,

$$\begin{gathered} N_1 < |\mathbb{S}| < N_2, \quad N_1, N_2 \in \Omega \\ \mathbb{S} \leftarrow \{s_i \big| (s_i = rand \in \Omega) \ \wedge (s_i \neq s_j \ \forall \ i \neq j)\} \end{gathered} \tag{17}$$

where the notation *rand* means a number chosen uniformly at random (i.e. $rand \sim U(\{N_1, N_1+1, ..., N_2-1, N_2\})$. Given the choice of $\mathbb{S}$, the optimal coefficients c_n were determined at each time and the objective function was evaluated. The set which yielded the lowest value of the objective was then selected as the optimal in stage 1. We call this set $\mathbb{S}_1$.

The second stage served as a "refinement" stage, in which the set $\mathbb{S}_1$ was perturbed and the objective was evaluated. Perturbations included the following: (i) a few modes were added or removed from $\mathbb{S}$, (ii) some or all of the modes in $\mathbb{S}$ were altered slightly. Mathematically, both procedures fall into the below operations or their combination.

$$\begin{gathered} \mathbb{S} \leftarrow \mathbb{S}_1 \cup \mathbb{S}_p, \ \ \mathbb{S}_p = \{s_i \big| s_i \in \Omega \backslash \mathbb{S}_1 \wedge |s_i - x_j| < a \ , x_j \in \mathbb{S}_1\} \\ \mathbb{S} \leftarrow \mathbb{S}_1 \cup \mathbb{S}_p, \ \ \mathbb{S}_p = \{s_i \big| s_i \in \Omega \ \wedge s_i \notin \mathbb{S}_1\} \\ \mathbb{S} \leftarrow \mathbb{S}_1 \backslash \mathbb{S}_p, \ \ \mathbb{S}_p \subset \mathbb{S}_1 \end{gathered} \tag{18}$$

The final set which yielded the lowest value of the objective function was then selected as the optimum. A pseudocode for the optimization routine is included in Appendix A. We note that to ensure convergence to a final set the algorithm was performed with 10 restarts.

RESULTS AND DISCUSSION

In this section we present the motion reconstructions and validate the models obtained after applying our methodology to the experimental data. We underscore that reconstruction of the motion using sequential modes (i.e. $\mathbb{S} = \{1,2,3,...N\}$) was attempted and yielded unreasonably high amplitudes even after removing low modes which are known to be sensitive to noise (Mukundan et al., 2010). Equation 11 was necessary to select and objectively compare between different mode choices while satisfying VIV constraints.

Convergence and computational cost

Although the stochastic optimization algorithm lacks theoretical convergence and global optimality guarantees, in practice convergence has been always observed. Specifically, after performing the algorithm with 10 restarts and performing 20,000 iterations with the last 1,000 iterations as the refinement stage, the returned set is the exact same for all 10 times.

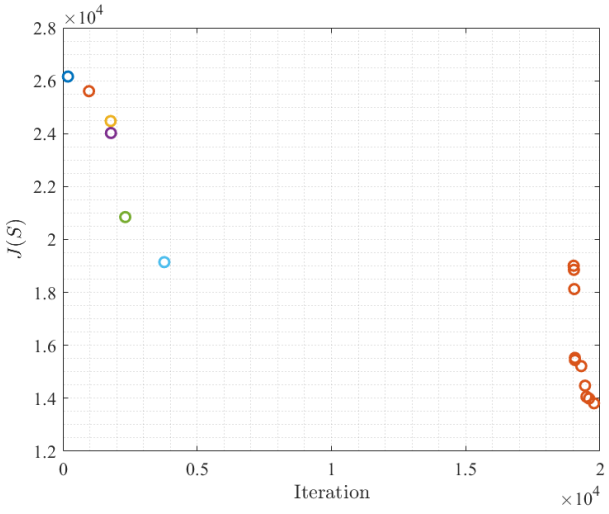

Fig. 1 Objective function plotted against iteration.

A typical plot of the objective function plotted against iteration is shown in Figure 1. We note that since the objective is not monotonically decreasing with iteration number, the value of the objective was only plotted if it was better than the previous best estimate. The first 19,000 iterations served as the exploration stage; we observe that the best set found in the exploration stage was found typically in less than 5,000 iterations. Rapid improvement to the final optimum was observed in the refinement stage (last 1,000 iterations).

The wall time required for the optimization algorithm to run is less than one hour, with 10 restarts, using a local workstation machine.

Reconstructed motion

Having learned the optimal mode set and time varying coefficient functions, we can reconstruct the motion of the riser using Equation 1.

The response of the riser as well as the average incident current profile are shown in Figure 2.

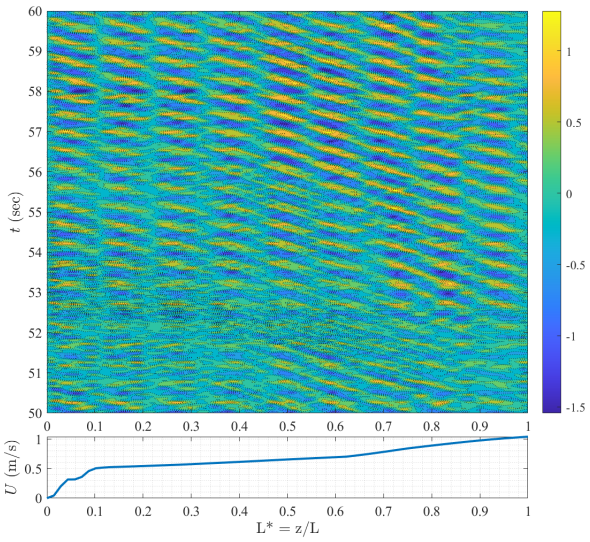

Fig. 2 Reconstructed riser motions (top) with the average normal incident current (bottom). The riser's span is measured on the x-axis while time is measured on the y-axis; the riser's displacement is highlighted as a contour plot on the plane, normalized by the riser's diameter. Any line parallel to the x-axis shows a "snapshot" of the riser in time. The riser is observed vibrating at the ninth mode with a frequency of about 2 Hz. A strong travelling wave response is recorded with waves travelling from the bottom end of the riser towards the top.

Figure 2 illustrates the riser's vibrations in time. The riser's span is measured on the x-axis, time is measured on the y-axis, while the displacement normalized by the riser's diameter is highlighted on the plane as a contour plot. The riser is observed vibrating in the ninth mode with amplitude of approximately one diameter and not exceeding approximately 1.5 diameters. A travelling wave response is evident with waves propagating from the bottom end of the riser, where the incident current was maximum, towards the top end of the riser, where the current was minimum. The result remains sensible while conforming to expected VIV physics-based constraints. The Strouhal frequency, which equals the vibration frequency is approximately, $f_{strouhal} \approx 2$ Hz.

Validation and Generalization

This section assesses quantitatively the validity of the obtained models by comparing them to experimental measurements, as well as how well the proposed methodology can generalize and perform on unseen data.

Root-mean-square motions

To validate the model, the root-mean-square (RMS) of the predicted motion was compared with observations. The results obtained for the RMS motion reconstruction and strain model predictions are shown in Figure 3. The top sub-figure shows the RMS amplitude (normalized by the diameter) as a function of span and the bottom sub-figure illustrates the RMS measured strain from the experiments as well as the strain reconstruction.

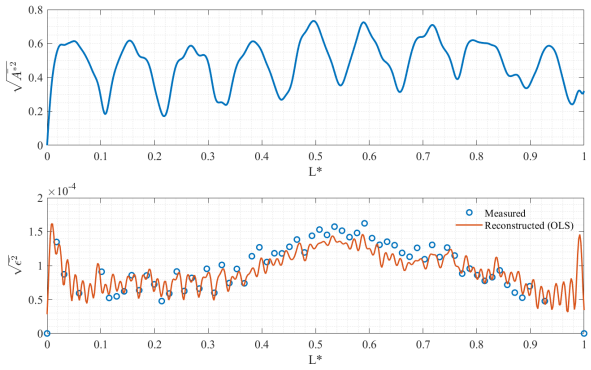

Fig. 3 RMS of riser's displacement (top) and RMS of riser's strain (bottom) as functions of span. The displacement plot shows a flexible body vibrating in the ninth mode. The reconstructed strain shows reasonable agreement with the measured values.

As is evident in Figure 3, the RMS displacement qualitatively agrees with the RMS vibration of a flexible body oscillating in the ninth mode (Rao, 1995). In addition, the reconstructed RMS strain values approximate the measurements' shape and magnitude to reasonable accuracy.

Cross-validation

To assess how well the learned model generalizes, a five-fold cross validation was performed. Specifically, 8 seconds of the total 10 seconds of available data were used to train the model each time and testing was done on the unseen two seconds. We include cross validation plots for training for the first 8 seconds and testing on the final 2 seconds. Figure 4 illustrates the predicted RMS displacement (top) as well as the reconstructed RMS strain (bottom). Besides experimental strain measurements, two reconstructions are shown both for the strain measurements and for the amplitudes; the solid blue line corresponds to the partially trained model and the solid orange line corresponds to the fully trained model.

As is evident in Figure 4, not only are both models reasonably accurate, they are in addition consistent. The cross-validation performed suggests that the model can generalize reasonably well.

Framework Complexity given the training data

Given the model's cross-validation results, a meaningful question to ask would be how large the dataset must be to train the model using the proposed stochastic mode search algorithm successfully. In order to answer this question, attempts were made to predict the full dataset in time, while reducing the number of training points gradually. Specifically, from the 10 seconds of data available (505 time steps), only a percentage of the available data was selected uniformly across time to train the model. Figure 5 illustrates results of the model after training on only 10% of the available data (50 out of the 505 timesteps) sampled uniformly across time.

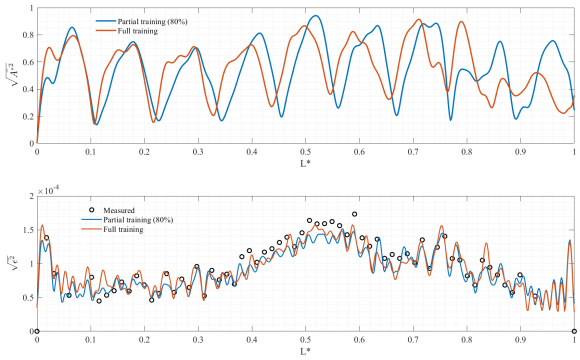

Fig. 4 RMS motion (top) and RMS strain (bottom) as functions of span. Reconstructions are shown of a model trained on all available data (orange), and of a model trained on 80% of available data (blue), which predicts unseen data.

As is evident in the figure, the results obtained by training on just a small subset of the data, 10% of the available, is almost indistinguishable from training on the full dataset. Not only does the algorithm perform reasonably well across the unseen time steps but also the results are very consistent with those obtained by training on the full dataset. This result is expected since the response is mostly periodic and thus a few representative samples should suffice for selecting the appropriate modes.

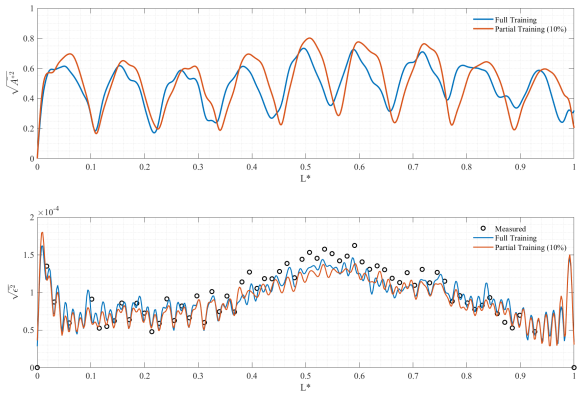

Fig. 5 RMS motion (top) and RMS strain (bottom) as functions of span. Reconstructions are shown of a model trained on all available data (orange) and a model trained on just 10% of available data (blue) sampled uniformly across time - which predicts unseen data 90% of the time. Predictions are reasonably accurate and consistent.

CONCLUSION

In this work, the VIV motions of a riser model were machine-learned from experimental strain data. A modal decomposition technique was augmented using machine-learning in order to infer a carefully selected set of expansion modes extracted directly from experimental data. The goal of the learning problem was to determine a sparse mode set capable of reasonably accurately predicting the motions while conforming to VIV physics-based constraints. The problem formulation provides specific conditions quantifying the reconstruction accuracy and demonstrates how the motions may be obtained by minimizing an appropriate objective.

Solving the learning problem requires optimizing a non-convex, non-smooth objective function with a variable number of unknown parameters subject to various constraints both essential (boundary conditions, amplitude modulation) and natural (generalized least squares optimality). In order to optimize the objective, the authors propose a stochastic mode search algorithm and demonstrate its capabilities and limitations. The optimization routine's convergence and computational cost are examined.

The results are validated using a five-fold cross-validation scheme and the framework's complexity in terms of data required for successful training is finally evaluated.

ACKNOWLEDGEMENTS

The authors would like to acknowledge support from the DigiMaR Consortium, MathWorks, and the Onassis Foundation.

In addition they would like to extend their gratitude to Professor J. Kim Vandiver and Dr. Vivek Jaiswal for generously open-sourcing the data from the MIAMI II experiments.

REFERENCES

Bernitsas, M. M., Ofuegbe, J., Chen, J.-U., and Sun, H. (2019). Eigensolution for flow induced oscillations (viv and galloping) revealed at the fluid-structure interface. In *ASME 2019 38th International Conference on Ocean, Offshore and Arctic Engineering*. American Society of Mechanical Engineers Digital Collection.

Guyon, I. and Elisseeff, A. (2003). An introduction to variable and feature selection. *Journal of Machine Learning Research*, 3:1157–1182.

Jaiswal, V. and Vandiver, J. K. (2007). Viv response prediction for long risers with variable damping. In *International Conference on Offshore Mechanics and Arctic Engineering*, volume 4269, pages 901–909.

Jhingran, V. and Vandiver, J. K. (2007). Incorporating the higher harmonics in viv fatigue predictions. In *International Conference on Offshore Mechanics and Arctic Engineering*, volume 4269, pages 891–899.

Marcollo, H., Chaurasia, H., and Vandiver, J. K. (2007). Phenomena observed in viv bare riser field tests. In *International Conference on Offshore Mechanics and Arctic Engineering*, volume 4269, pages 989–995.

Mukundan, H. (2008). Vortex-induced vibration of marine risers: motion and force reconstruction from field and experimental data. *Massachusetts Institute of Technology*.

Mukundan, H., Hover, F., and Triantafyllou, M. (2010). A systematic approach to riser viv response reconstruction. *Journal of fluids and structures*, 26(5):722–746.

Rao, S. S. (1995). Mechanical vibrations. *Addison Wesley Boston, MA*.

Swithenbank, S. B. and Vandiver, J. K. (2007). Identifying the power-in region for vortex-induced vibrations of long flexible cylinders. In *International Conference on Offshore Mechanics and Arctic Engineering*, volume 4269, pages 723–730.

Triantafyllou, M. S., Bourguet, R., Dahl, J., and Modarres-Sadeghi, Y. (2016). Vortex-induced vibrations. In *Springer Handbook of Ocean Engineering*, pages 819–850. Springer.

Triantafyllou, M. S., Triantafyllou, G. S., Tein, Y. S., and Ambrose, B. D. (1999). Pragmatic riser viv analysis. In *Offshore Tech. Conf.* Offshore Technology Conference.

Wang, J., Fu, S., Baarholm, R., Zhang, M., and Liu, C. (2019). Global motion reconstruction of a steel catenary riser under vessel motion. *Ships and Offshore Structures*, 14(5):442–456.

Williamson, C. and Roshko, A. (1988). Vortex formation in the wake of an oscillating cylinder. *Journal of Fluids and Structures*, 2(4):355–381.

Wu, W., Bernitsas, M. M., and Maki, K. (2014). Rans simulation versus experiments of flow induced motion of circular cylinder with passive turbulence control at 35,000 << 130,000. *Journal of Offshore Mechanics and Arctic Engineering*, 136(4).

Zdravkovich, M. (1996). Different modes of vortex shedding: an overview. *Journal of fluids and Structures*, 10(5):427–437.

ALGORITHMS

Algorithm 1 Stochastic Mode Search ($\boldsymbol{J}(\mathbb{S})$)

$\mathbb{S}_{best} \leftarrow$ *random set*
$\boldsymbol{J}_{best} \leftarrow +\infty$
for i = number of total iterations **do**
  if i in exploration stage **then**
    $\mathbb{S} \leftarrow$ *random set* $\subseteq \Omega$
  else if i in refinement stage **then**
    $\mathbb{S} \leftarrow$ *perturbation of* $\mathbb{S}_{best}$
  end if

  for t = recorded times **do**
    $c_n(t) \leftarrow \arg\min_{c_n} \sum_{z_i} (\mathrm{Y}''(z_i) - \frac{\varepsilon_{CF}(z_i,t)}{R})^2$
  end for

  if $\boldsymbol{J}(\mathbb{S}) < \boldsymbol{J}_{best}$ **then**
    $\boldsymbol{J}_{best} \leftarrow \boldsymbol{J}(\mathbb{S})$
    $\mathbb{S}_{best} \leftarrow \mathbb{S}$
  end if
end for
return $\mathbb{S}_{best}$

EXPLANATORY FIGURES

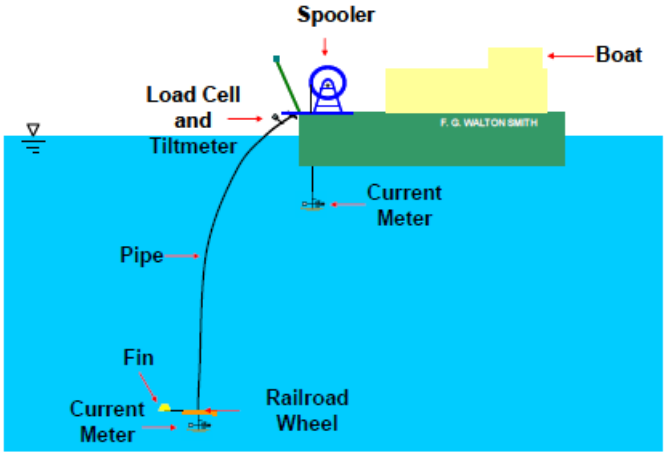

Fig. 6 Depiction of experimental setup. The riser model was towed behind vessel F.G. Walton Smith. This illustration is not drawn to scale and is for visualization purposes only. [provided by Prof. J.K. Vandiver, MIT]